Instrument Science Report WFC3 2007-10

WFC3 Ambient Testing: UVIS Dark Current Rate

B. Hilbert
April 27, 2007

ABSTRACT

Ground testing of WFC3 under ambient conditions during April of 2007 was performed in order to prepare for upcoming thermal vacuum testing. As a part of this ambient testing, the dark current rate of the spare UVIS package (UVIS build 2) was measured while the CCD was operating at a temperature of -54°C. This temperature is significantly higher than the nominal operating temperature of -83°C, leading to a higher overall dark current rate, as well as a larger population in the high dark current tail of the distribution. Measured dark current values at the peak of the distributions corresponding to the 4 amplifiers were 9.0 – 13.9 e^-/pix/hour.

Introduction

In preparation for WFC3's upcoming thermal vacuum testing, the instrument underwent ground testing under ambient conditions during April of 2007. Testing was performed at NASA's Goddard Space Flight Center. This testing provided the first opportunity to collect calibration data with the UVIS-2 (flight spare) detector package in the instrument.

During the ambient testing, the operating temperature of the UVIS detector was roughly -54°C. This is warmer than the nominal operating temperature by 29°C, and also warmer than the temperature used during previous ambient testing. As dark current levels in the UVIS detectors are dependent upon operating temperature, one of the first datasets acquired during the ambient testing was designed to measure the dark current.

Data

Data were collected under the dark current SMS UV01S01A. This SMS contained 4 bias images and 2 dark current images. The details of these exposures are listed in Table 1. In addition to these images, the dark current rate was measured in two 1000-second dark current images from the UVIS Science Monitor SMS, UV28S01.

Filename	***Entry Number***	***Exposure Time (sec)***	***Exposure Type***	***Detector Temperature (^oC)***
iu011a01r_07105082051	28388	0	bias	-54.26
iu011a02r_07105082051	28389	0	bias	-54.05
iu011a04r_07105085255	28390	1000	dark	-53.63
iu011a05r_07105085255	28391	0	bias	-54.05
iu011a07r_07105095907	28392	3000	dark	-54.05
iu011a08r_07105095907	28393	0	bias	-54.05
iu281c09r_07105044535*	28366	1000	dark	-54.26
iu281d09r_07110004635*	29018	1000	dark	-54.05

*Table 1 Data used to calculate the UVIS ambient testing dark rate. Filenames are for files after having been processed through OPUS. Entry numbers correspond to image ID numbers during the ambient testing. * Files were part of the UVIS Science Monitor SMS.*

Analysis

Before dark current calculations could be made, several data reduction steps were performed. First, overscan pixel values were subtracted from each image. The subtracted values were derived using the serial virtual overscan pixels. For each row on the detector, the median value of the serial virtual overscan pixels was calculated. We then fit a line across the rows, to these median values. The value of the best-fit line in each row was subtracted from the science pixels in that row. For a better description of these overscan pixels, see Howard Bushouse's ISR on the CCD overscan layout (ISR 2003-14). For this study, we follow the previously defined convention for the named quadrants of the detector. Amps A and B are located in the upper left and right corners of the detector. Amps C and D occupy the bottom left and right corners, respectively.

After overscan subtraction, the four bias images listed in Table 1 were combined to create a mean bias image. This bias image was subtracted from the four overscan subtracted dark current images. Analysis of gain data taken during ambient testing revealed gain values for the A, B, C, and D quadrants of the UVIS detector of 1.58, 1.55, 1.65, and 1.61 e^-/DN respectively (S. Baggett, private comm.). These gain values were applied to the dark current images, to convert counts to electrons.

Histograms of the dark current values calculated for the 3000-second exposure are shown in Figure 1. As expected, the elevated operating temperature of the CCDs produced a tail of high dark current pixels larger than that observed in previous ambient and thermal vacuum testing. (Hilbert and Baggett, 2005 and Hilbert and Baggett, 2004.) In an attempt to limit the effects of the high dark current tail on the statistics, the distribution in each quadrant was sigma clipped 3 times at the 3-σ level. Histograms of the sigma clipped distributions for the 3000-second exposure are shown in Figure 2. In all cases, a significant high dark current tail remained. Gaussian fits to these clipped distributions also failed to aid in the characterization of the dark current. Neglecting the extended dark current tail, the measured dark current distributions remained not-quite Gaussian. Fitted Gaussian peaks deviated significantly enough from the measured peaks of the distributions as to be useless as measures of dark current. As a result, dark currents were instead characterized using three simple measurements: the value of the peak of the dark current distribution, the mean dark current level and the standard deviation of the distribution.

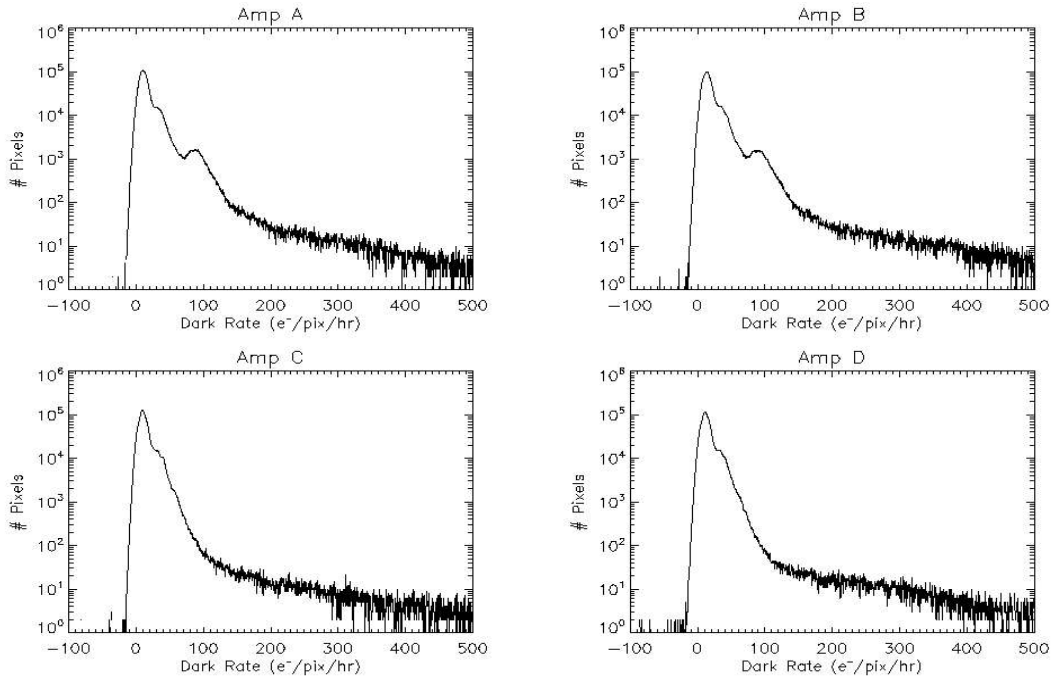

Illustration 1 Dark current histograms of the four quadrants of the CCD for the 3000-second exposure prior to sigma clipping. The tail of high dark current pixels extends farther than in previous ambient and thermal vacuum testing, due to a higher CCD temperature.

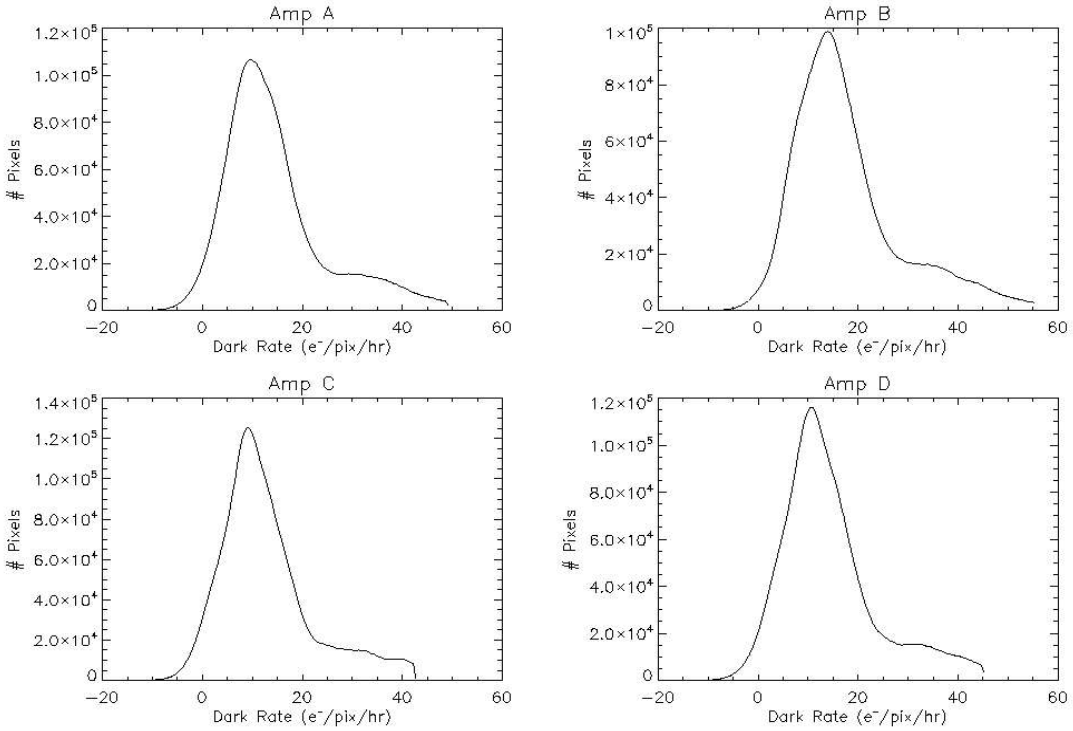

Illustration 2 Histograms of the sigma-clipped 3000-second dark current image. Significant high dark current tails remain.

Results: 3000-second exposure

Figures 1 and 2 show histograms of the dark current distributions for the 3000 second image before and after sigma clipping. While sigma clipping removed some of the high dark current tail, a significant population of high dark current pixels remained. Table 2 gives the dark current measurements made on the sigma clipped image. The difference between the peak and the mean dark current values gives an idea of the extent of the high dark current tail in the distribution.

	Dark Current Peak (e⁻/pix/hr)	***Mean Dark Current (e⁻/pix/hr)***	***1-σ of Dark Distribution (e⁻/pix/hr)***
Amp A	9.8	12.9	10.2
Amp B	13.9	16.2	10.8
Amp C	9.0	11.9	9.3
Amp D	10.9	13.2	9.6

Table 2 Peaks in the dark current distributions, mean dark currents, and the standard deviation of the dark current distribution for the 3000 second dark image.

Results: 1000-second exposures

Figure 3 shows the sigma clipped dark current distributions for the three 1000-second exposures. Corresponding statistics are listed in Table 3. The higher relative noise associated with the shorter exposure time for these images did not allow the high dark rate pixels to distinguish themselves from the general population as well as in the 3000-second image. As a result, the histograms of the 1000-second images do not show the well defined high dark current tail tacked on to the edge of a nearly Gaussian distribution, as in Figure 2. Instead, the histograms in Figure 3 show wider distributions along their entire height.

Amps C and D, which together comprise chip 2, also both show a “shoulder” to their histograms that isn't apparent in the Amp A and B histograms. The position of this shoulder at 25-30 e-/pix/hour matches that of the edge of the high dark current tail seen in Figure 2, and suggests that the population of pixels in this shoulder becomes the dark current tail seen in Figure 2.

Also, the dark current image taken during the Science Monitor SMS at the beginning of ambient testing (iu281c09r_07105044535) shows dark current histograms shifted to slightly lower values than in the other dark current images. The detector

temperature during this exposure was colder by 0.2°C and 0.6°C than during the other two 1000-second exposures. However, nearly identical dark current distributions in those other two exposures, despite a temperature difference of 0.4°C, suggests that temperature differences of this magnitude are not significant, and that there must be another cause behind the shifted dark current distribution.

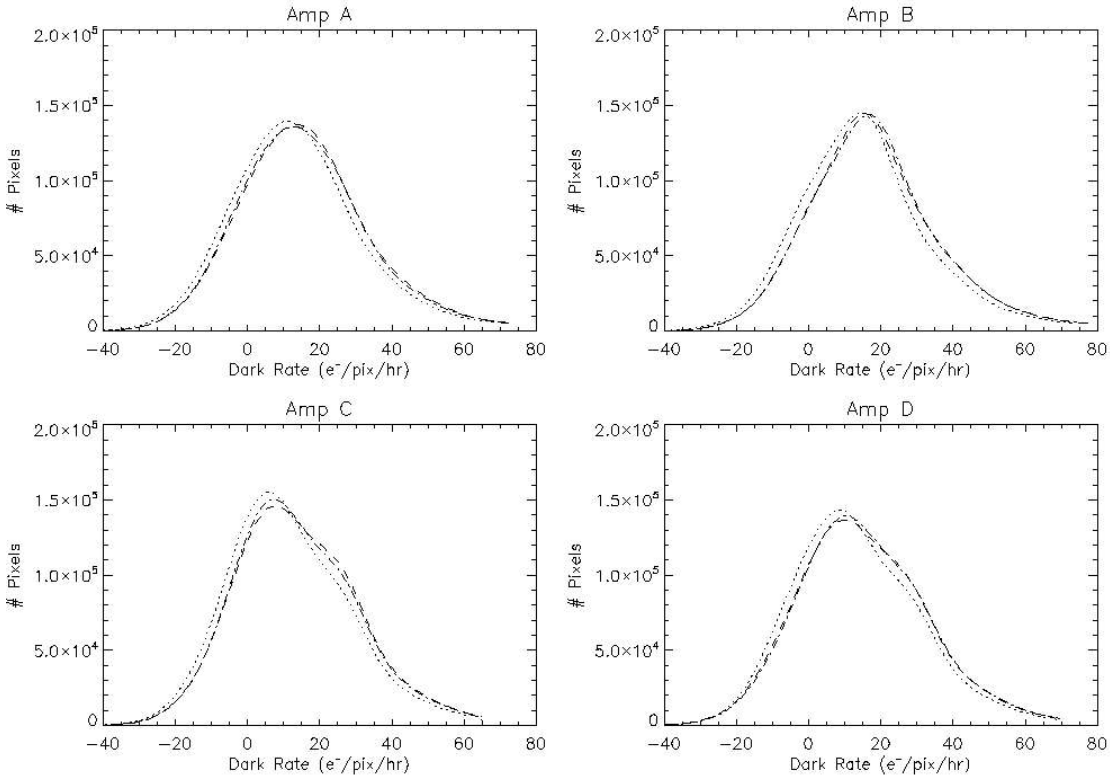

Illustration 3 Dark current histograms for the sigma-clipped 1000-second exposures. The high dark current tails are not as apparent in these distributions due to the shorter exposure time. Note that one of the images, associated with the Science Monitor run at the beginning of ambient testing (dotted line), shows a slightly lower dark current in all quadrants compared to the other two images.

	Dark Current Peak (e^-/pix/hr)	*Mean Dark Current (e^-/pix/hr)*	*1-σ of Dark Distribution (e^-/pix/hr)*
iu011a04r_07105085255			
Amp A	13.6	15.1	17.9
Amp B	16.1	17.8	18.2
Amp C	7.3	13.3	16.9
Amp D	10.1	15.3	17.8
iu281c09r_07105044535			
Amp A	10.8	13.4	17.6
Amp B	14.3	15.0	17.7
Amp C	6.5	11.3	16.6
Amp D	8.9	13.2	17.3
iu281d09r_07110004635			
Amp A	14.0	15.6	17.9
Amp B	15.4	18.0	18.1
Amp C	8.4	13.9	17.0
Amp D	10.0	15.7	17.8

Table 3 Peaks in the dark current distributions, mean dark currents, and the standard deviation of the dark current distribution for the 1000 second dark images.

A mean dark current image was constructed using the three 1000-second images, in an effort to reduce the noise of the dark current distribution. Histograms of each quadrant of the mean image are plotted in Figure 4, and corresponding statistics are listed in Table 4. The width of this mean distribution is still larger than that of the single 3000-second image.

	Dark Current Peak (e^-/pix/hr)	*Mean Dark Current (e^-/pix/hr)*	*1-σ of Dark Distribution (e^-/pix/hr)*
Amp A	11.0	14.2	13.3
Amp B	13.0	16.4	13.7
Amp C	8.9	12.5	12.5
Amp D	10.6	14.4	13.1

Table 4 Dark current statistics for the mean image, constructed from all three 1000-second exposures.

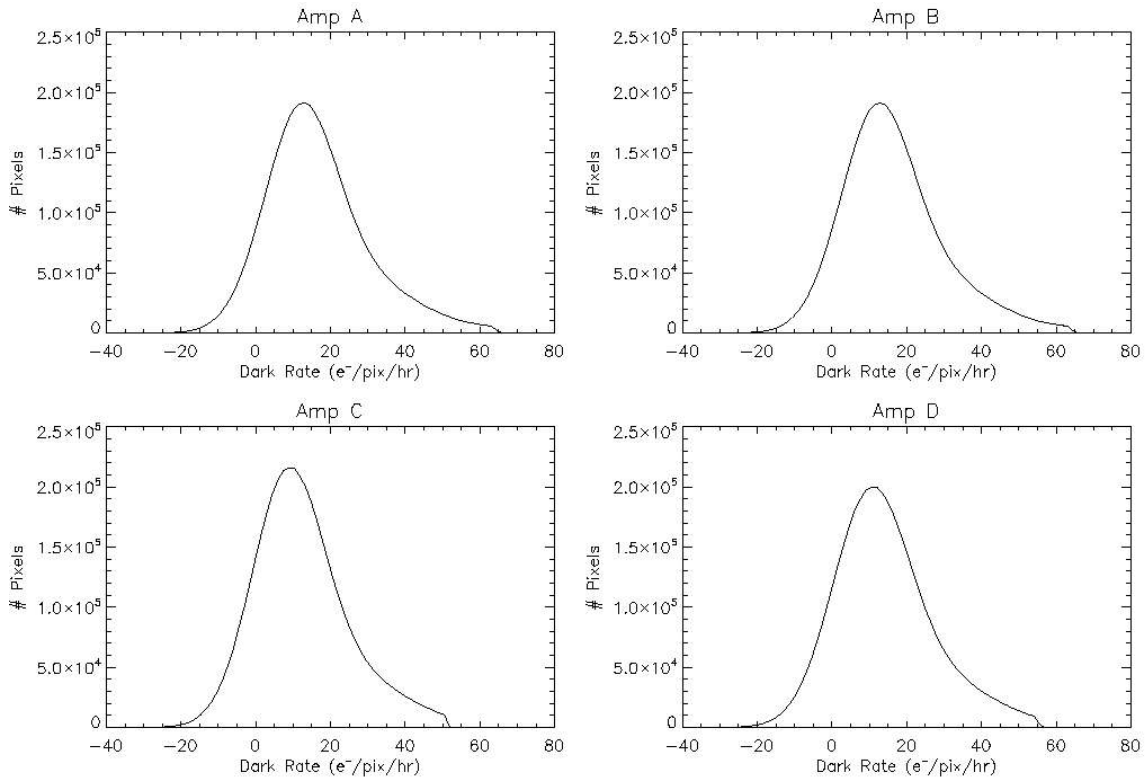

Illustration 4 Dark current histograms for the mean image, constructed from the three 1000-second images.

Conclusions

Using the peak of the dark current distribution as a representative measure of the dark current in one quadrant of the UVIS detector, we measure dark currents between 9.0 and 13.9 e^-/pix/hour. Quadrant B consistently shows an elevated dark current relative to the other quadrants, while quadrant C shows the lowest dark current. With their more sharply peaked distributions, high dark current tails have a larger effect on quadrant C and D statistics, compared to quadrants A and B, as seen in the difference between peak and mean dark current values.

References

Bushouse, H., ***WFC3 UVIS CCD Image Overscan Region Layouts***. ISR WFC3-2003-14. http://www.stsci.edu/hst/wfc3/documents/ISRs 9 December 2003.

Hilbert, B. and S. Baggett, ***WFC3 UVIS Dark Current and Readnoise from Ambient Testing***. ISR WFC3-2004-13. http://www.stsci.edu/hst/wfc3/documents/ISRs 10 August, 2004.

Hilbert, B. and S. Baggett, ***Results of WFC3 Thermal Vacuum Testing – UVIS Readnoise and Dark Current***. ISR WFC3-2005-13. http://www.stsci.edu/hst/wfc3/documents/ISRs 28 March 2005.